Blazar origin of the UHECRs and perspectives for the detection of astrophysical source neutrinos at EeV energies

Xavier Rodrigues,* Jonas Heinze,† Andrea Palladino,‡ Arjen van Vliet,§ and Walter Winter¶
DESY, Platanenallee 6, 15738 Zeuthen, Germany
(Dated: March 20, 2020)

We demonstrate that a population of blazars can describe the observed spectrum and composition of Ultra-High-Energy Cosmic Rays (UHECRs), and that the dominant contribution comes from low-luminosity BL Lacs. However, a sub-dominant contribution from high-luminosity blazars can lead to a substantial neutrino flux which will peak at EeV energies. We find that it is plausible that this neutrino flux from the sources outshines the cosmogenic neutrino flux produced during the propagation of UHECRs. This has profound implications for the high-energy (EeV) neutrino detection experiments: their main target may be source neutrinos, for which additional search strategies can be used, such as stacking searches, flare analyses, or multi-messenger follow-ups.

arXiv:2003.08392v1 [astro-ph.HE] 18 Mar 2020

Blazars are Active Galactic Nuclei (AGN) with their jets pointed towards Earth; they contribute more than 80% of the Extragalactic Gamma-ray Background (EGB) [1], dominating the gamma-ray emission above 50 GeV. In addition, there are strong indications for correlations in arrival directions of UHECRs with extragalactic gamma-ray sources, including AGN [2]. Blazars are also one of the candidate classes which may have sufficient power to maintain the UHECR flux. As a consequence, it is natural to consider blazars as possible origin of the observed UHECRs.

On the other hand, a diffuse flux of high-energy astrophysical neutrinos has been discovered [3]. This may be a direct indicator for the origin of UHECRs because neutrinos point back directly to their sources, while UHECRs are deflected by (Galactic and extragalactic) magnetic fields. The recent detection of neutrinos from the flaring blazar TXS 0506+056 provides further evidence that cosmic rays are accelerated in blazars [4, 5], see also earlier results [6]. However, dedicated experimental searches for neutrinos from known objects in catalogues limit the contribution of these objects to below about 20% [7]. This means that observable gamma-ray blazars are probably not the dominant source of neutrinos at TeV-PeV energies. At the same time, it cannot be excluded that neutrino sources at EeV ($\sim 10^{18}\,\mathrm{eV} = 10^{9}\,\mathrm{GeV}$) energies exist, where currently only upper limits are placed [8, 9]. Indeed, if blazars significantly contribute to the UHECRs flux, they will need to accelerate protons and cosmic-ray nuclei up to $\sim 10^{20}$ eV. The neutrinos from AGN are expected to carry a fraction of the primary energy, $\simeq 0.05\,E_p$ for protons, which means that a significant neutrino flux is expected in the EeV energy range.

Cosmogenic neutrinos are neutrinos produced in UHECR interactions during their propagation over extragalactic distances. They are the main target for radio-detection neutrino experiments in the EeV range such as the radio array of IceCube-Gen2 [10], GRAND [11], ARA [12] and ARIANNA [13]. Recent descriptions of the UHECR spectrum and composition, however, indicate that the maximum energies are limited by the accelerators; they can be described by a rigidity-dependent maximum energy $E_{\mathrm{CR}} \propto Z$ with Z the charge of the nucleus [14]. Such an energy dependence is, for instance, generated if the Larmor radius of a particle is to be confined within a certain region of fixed size. This framework, however, implies very small cosmogenic neutrino fluxes [15, 16], although a potential significant contribution to the neutrino flux from a sub-dominant proton population is tolerable by data [17]. In this letter we scrutinize the hypothesis that the EeV neutrino sky is dominated by cosmogenic neutrinos, and we demonstrate that source neutrinos may be the foreground.

The production of UHECRs or neutrinos in blazars has been studied in previous works (see *e.g.* Refs. [18–21]). However, a self-consistent description of the UHECR spectrum and composition including a neutrino flux prediction from the AGN population has so far been missing. Furthermore, most EeV neutrino source models lack the motivation for such high cosmic ray energies. This motivation could be either that data on the UHECR spectrum and composition are well described (such as in Refs. [22–24] for other source classes), or that a description for particle acceleration to UHECR energies exists (e.g. Refs. [25, 26] for AGN) – whereas normally *ad hoc* assumptions for the maximum energy (or acceleration efficiency) are made. The model in this work satisfies both criteria, as we employ recent results based on numerical simulations that suggest that cosmic rays in AGNs can be re-accelerated by the jet to energies as high as 10^{20} eV [26]. We also adopt the composition of accelerated cosmic rays suggested in that work, which strongly constrains our model's flexibility to describe UHECR data. We also combine different populations of blazars: low-luminosity BL Lacs, high-luminosity BL Lacs, and Flat-Spectrum Radio Quasars (FSRQs), each with different characteristics. Compared to an earlier work [27], the purpose here is to describe UHECR data and study the implications for the neutrino fluxes instead of describing PeV neutrino data (which requires much lower cosmic-ray acceleration energies).

We simulate sources (blazars) and UHECR propagation in a combined source-propagation model. It has three ingredients: simulation of photo-hadronic processes of UHE-

*Electronic address: xavier.rodrigues@desy.de
†Electronic address: jonas.heinze@desy.de
‡Electronic address: andrea.palladino@desy.de
§Electronic address: arjen.van.vliet@desy.de
¶Electronic address: walter.winter@desy.de

CRs in blazar jets; simulation of the propagation of the escaping cosmic rays towards Earth, including cosmogenic neutrino production; comparison of the diffuse UHECR and neutrino fluxes from the entire blazar population with measured observables. Here, we sketch the basic ingredients of our model, and we refer to Appendix A for details.

A mechanism that is capable of re-accelerating cosmic rays in blazar jets up to energies of ~ 100 EeV has been suggested recently [26]. The accelerated UHECRs will interact with target photons in the jet, leading to photodisintegration and photo-pion production. The latter process leads to the emission of neutrinos, which, in environments with moderate magnetic fields such as blazars, will have energies that follow the energy of the primary nuclei. We simulate these radiative processes in blazar jets numerically, using the NeuCosmA code [28, 29] and the blazar model introduced in Ref. [20]. For BL Lacs, we use a one-zone model where the cosmic rays interact with the non-thermal radiation produced in the jet. For FSRQs, photons emitted from the broad line region and the dust torus provide additional targets for the photo-hadronic interactions, which enhance the neutrino emission.

Following Ref. [26], we consider a fixed mass composition of the accelerated cosmic rays, which consists of a mixture of four mass groups: protons, helium-4, nitrogen-14 and iron-56, with relative abundances [1, 0.46, 0.30, 0.14], respectively, which roughly follows the Galactic cosmic-ray composition. The maximum energy of each of these four mass groups is determined self-consistently; it is the energy at which the particle's energy losses become more efficient than the acceleration. Evidently, this depends on the luminosity of each blazar and on the magnetic field strength in the jet, as detailed in Appendix A. The spectrum following target photons in the jet is adopted from the so-called *blazar sequence* [30, 31], an assumption used in previous multi-messenger studies of blazars [19, 20]. These spectra are based on an average of multi-wavelength blazar observations, and are assumed to depend only on the blazar's gamma-ray luminosity, L_γ. Specifically, brighter blazars exhibit non-thermal broadband emission at lower frequencies. The hadronic interactions of the accelerated isotopes with this static photon field leads to a nuclear cascade of lighter species, each of which is treated self-consistently throughout the simulation. The mechanism by which the cosmic rays escape the jet will also influence the emitted cosmic-ray spectrum and composition; see Appendix A. It allows for a relatively hard emission spectral index, which is necessary to be able to fit the measured UHECR spectrum and composition at Earth (see e.g. [14, 16]).

We combine individual blazars from three populations to estimate the contribution from the entire blazar population, for which we adopt the cosmological blazar evolution model by Ajello *et al.* [32, 33]. This model is illustrated in Fig. 1 as a function of redshift and gamma-ray luminosity; it was created to describe the diffuse gamma-ray flux. For example, FSRQs are (on average) brighter in gamma rays, making them the most efficient neutrino-emitting blazars [20]. Low-luminosity BL Lacs, on the other hand, have the highest efficiency in UHECR emission of all blazar subclasses, since the low photon densities in the jet allow the survival and escape of the accelerated nuclei. Additionally, this source class is expected to have a strong negative cosmological evolution (most sources have a redshift $z < 0.5$ as shown in Fig. 1), which further minimizes cosmic-ray energy losses during propagation.

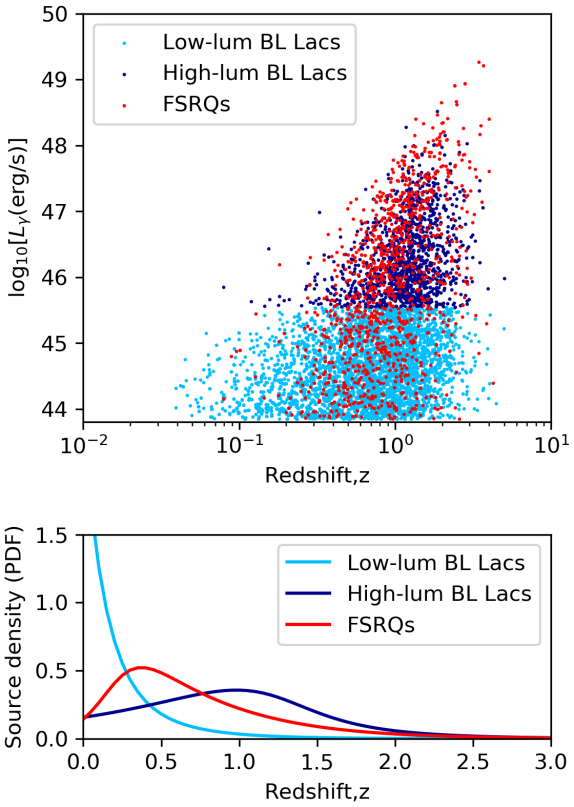

FIG. 1: Representation of the blazar population as a function of redshift and luminosity, following Ajello *et al.* [32, 33]. Here we divide blazars into FSRQs, low-luminosity BL Lacs, and high-luminosity BL Lacs. The lower panel shows the same distribution in redshift (integrated over luminosity) and it clearly shows the strong negative evolution of low-luminosity BL Lacs compared with other blazars.

We then calculate the extragalactic propagation of UHECRs from this blazar population until Earth using the novel numerical code PriNCe [16]. Photo-hadronic interactions with the extragalactic background light (EBL) and the cosmic microwave background (CMB) lead to the cooling of the cosmic rays during propagation, as well as the creation of lighter elements and the emission of cosmogenic neutrinos. Cosmic expansion additionally leads to the adiabatic cooling of the cosmic rays.

The source-propagation model has been applied to a wide range of values of four blazar properties: baryonic loading, acceleration efficiency, cosmic-ray escape mechanism and size of the production region (see Appendix A), which can each have different values for low-luminosity BL Lacs, high-luminosity BL Lacs, and FSRQs. Other model parameters, such as the relative abundances of the accelerated cosmic rays, have been fixed. This choice increases the predictive

power of the model, at the expense of freedom in describing UHECR data, and it limits the computational effort. The objective of the parameter scan has been twofold: *(a)* to investigate how well the blazar population can explain the UHECR spectrum observed by the Pierre Auger Observatory (henceforth, *Auger*) [34], as well as the air shower measurements indicative of the mass composition of UHECRs [35]; and *(b)* to study what the minimum and maximum expected fluxes of both source and cosmogenic neutrinos are, particularly in the EeV range – while the current IceCube limits at lower energies are to be obeyed [7].

We present our main result describing UHECR spectrum and composition together with the predicted neutrino fluxes in Fig. 2 – see Appendix B for how we come to this conclusion for the combination of the different blazar populations. Although this result captures the general tendency of a heavier composition with energy, the data points are not extremely well described because the original composition of the accelerated cosmic-rays has not been optimized, but was instead fixed to a composition motivated by Ref. [26].

In the upper left panel, we demonstrate that it is possible to interpret the shape of the UHECRs flux (at and above the ankle) with a dominant contribution from low-luminosity BL Lacs. On the other hand, these objects do not provide a relevant contribution to the high-energy neutrino flux (see upper right panel). Neutrino production is relatively inefficient in these sources because of low target-photon densities, which means that the neutrino flux is dominated by cosmogenic neutrinos.

However, high-energy neutrinos are efficiently produced in high-luminosity blazars, such as FSRQs, where the photon density is high. In this case the neutrino flux is predominantly constrained by the upper limits provided by IceCube – and less by the cosmic-ray data. Indeed, FSRQs give a small contribution to the UHECRs flux, at a level of 10% above EeV energies, although this contribution does improve the composition observables. Therefore, the neutrino flux from FSRQs is not guaranteed, and can only be regarded as a (viable) possibility.

From the upper right panel we see that the neutrino flux from sources is (in the best case) higher than the cosmogenic neutrino flux. This is a very important result, since the next generation of EeV neutrino telescopes has been designed for the purpose to detect cosmogenic neutrinos. However, in the scenario illustrated above, high-energy neutrinos from FSRQs might be the foreground and cosmogenic neutrinos the background. It is important to remember that cosmogenic neutrinos are isotropically distributed, while source neutrinos point directly to the sources, which allows for different detection techniques, such as stacking searches, flare analyses or multi-messenger follow-ups. It is also interesting that the sources may even contribute a few events at PeV energies, but the predicted flux is well below the current stacking limit.

In Fig. 3 we represent the possible ranges for source neutrinos (blue band) and cosmogenic neutrinos (brown band) inferred from our analysis. The most optimistic case for source neutrinos corresponds to the right panel of Fig. 2. However, since the neutrino flux from FSRQs is not constrained by UHECRs, the flux can be lower. If FSRQs were purely leptonic sources, they would not contribute to the neutrino fluxes at all, and low-luminosity BL Lacs would dominate both neutrino fluxes. A minimum for the cosmogenic neutrino flux can be obtained when low-luminosity BL Lacs power the UHECRs flux – which is, however, difficult to detect with the future instruments currently proposed. The maximal cosmogenic neutrino flux has been obtained for the model dominated by high-luminosity BL Lacs in Appendix B, which may outshine the source neutrinos in that case. The question of whether cosmogenic neutrinos are foreground or background therefore depends somewhat on the model assumptions.

In summary, we have performed a self-consistent description of blazars as the sources of the UHECRs, including: a source model treating the nuclear cascade in the sources, an UHECR transport model, and a blazar population model describing the extragalactic gamma-ray background and the evolution of the spectral energy distribution. The acceleration model and expected injection composition have been well motivated from the literature.

We find that low-luminosity BL Lacs can describe the UHECR spectrum and composition, while the expected neutrino fluxes are low. However, we point out that a substantial contribution from high-luminosity BL Lacs and FSRQs, which does not dominate the UHECR description but does improve it, can lead to large source and cosmogenic neutrino fluxes within the reach of upcoming experiments.

We, furthermore, highlight that astrophysical source neutrinos from blazars may outshine the cosmogenic neutrino flux, which means that cosmogenic neutrinos could actually be the background and not the foreground at EeV neutrino energies. Since source neutrinos can be identified and disentangled with different techniques, such as stacking searches, flare analyses, or multi-messenger follow-up, this result has profound implications for the planning and analysis of future radio-detection experiments in the EeV range, and will open a new field of research. Note that the source neutrino flux spans over many orders of magnitude in energy, even combined analysis between TeV-PeV and EeV neutrino experiments will be of great interest.

Acknowledgments. The authors would like to thank Anna Franckowiak and Anna Nelles for comments on the manuscript. This project has received funding from the European Research Council (ERC) under the European Union's Horizon 2020 research and innovation programme (Grant No. 646623). XR was supported by the Initiative and Networking Fund of the Helmholtz Association.

[1] M. Ackermann *et al.* (Fermi-LAT), Phys. Rev. Lett. **116**, 151105 (2016), arXiv:1511.00693 [astro-ph.CO].
[2] A. Aab *et al.* (Pierre Auger), Astrophys. J. **853**, L29 (2018), arXiv:1801.06160 [astro-ph.HE].
[3] M. G. Aartsen *et al.* (IceCube), Science **342**, 1242856 (2013), arXiv:1311.5238 [astro-ph.HE].
[4] M. G. Aartsen *et al.* (Liverpool Telescope, MAGIC,

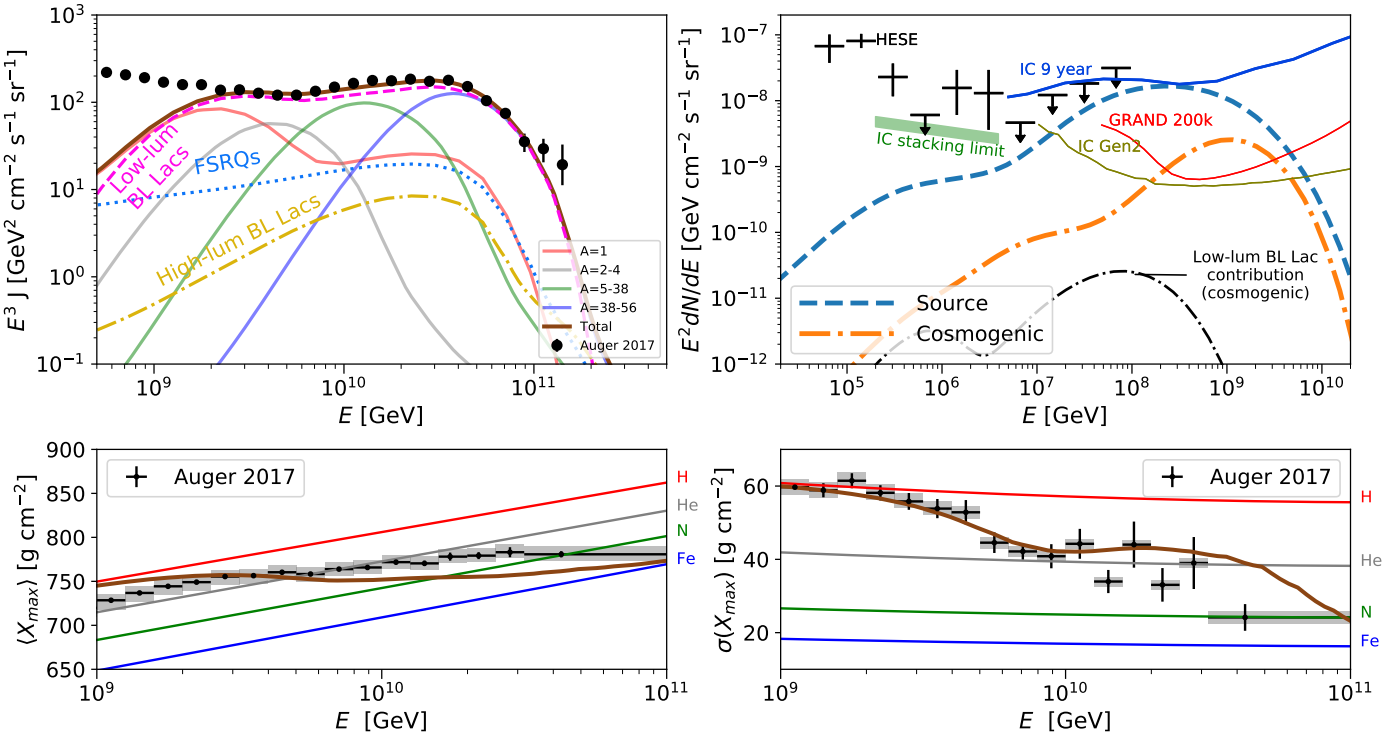

FIG. 2: Description of UHECR spectrum and composition as well as predicted neutrino fluxes. *Top left:* Simulated UHECR spectrum from the entire blazar population (dominated by low-luminosity BL Lacs), compared to data from the Pierre Auger Observatory [34]. *Top right:* maximum (all-flavor) diffuse neutrino flux (dominated by FSRQs) that can be obtained self-consistently without violating current IceCube observations, namely the flux of HESE events (black, [36]), the stacking limit for blazars assuming a spectral index of 2.2 (green band, [7]), and the upper limits up to extremely high energies (blue curve, [8]). Also shown are the expected sensitivities of the future radio array of IceCube-Gen2 (olive green, [10]) and of the planned radio neutrino detector GRAND [11]. The two bottom panels show the average *(bottom left)* and standard deviation *(bottom right)* of the depth of the cosmic-ray shower maximum, $X_{\rm max}$, compared to Auger measurements [35]. The colored lines correspond to the values expected for different isotopes according to the Epos-LHC air shower model [35].

H.E.S.S., AGILE, Kiso, VLA/17B-403, INTEGRAL, Kapteyn, Subaru, HAWC, Fermi-LAT, ASAS-SN, VERITAS, Kanata, IceCube, Swift NuSTAR), Science **361**, eaat1378 (2018), arXiv:1807.08816 [astro-ph.HE].

[5] M. G. Aartsen *et al.* (IceCube), Science **361**, 147 (2018), arXiv:1807.08794 [astro-ph.HE].

[6] M. Kadler *et al.*, Nature Phys. **12**, 807 (2016), arXiv:1602.02012 [astro-ph.HE].

[7] M. G. Aartsen *et al.* (IceCube), Astrophys. J. **835**, 45 (2017), arXiv:1611.03874 [astro-ph.HE].

[8] M. G. Aartsen *et al.* (IceCube), Phys. Rev. **D98**, 062003 (2018), arXiv:1807.01820 [astro-ph.HE].

[9] A. Aab *et al.* (Pierre Auger), JCAP **1910**, 022 (2019), arXiv:1906.07422 [astro-ph.HE].

[10] M. G. Aartsen *et al.* (IceCube), (2019), arXiv:1911.02561 [astro-ph.HE].

[11] J. Álvarez Muñiz *et al.* (GRAND), Sci. China Phys. Mech. Astron. **63**, 219501 (2020), arXiv:1810.09994 [astro-ph.HE].

[12] P. Allison *et al.*, Astropart. Phys. **35**, 457 (2012), arXiv:1105.2854 [astro-ph.IM].

[13] S. W. Barwick *et al.* (ARIANNA), Astropart. Phys. **70**, 12 (2015), arXiv:1410.7352 [astro-ph.HE].

[14] A. Aab *et al.* (Pierre Auger), JCAP **1704**, 038 (2017), arXiv:1612.07155 [astro-ph.HE].

[15] R. Alves Batista, R. M. de Almeida, B. Lago, and K. Kotera, JCAP **1901**, 002 (2019), arXiv:1806.10879 [astro-ph.HE].

[16] J. Heinze, A. Fedynitch, D. Boncioli, and W. Winter, Astrophys. J. **873**, 88 (2019), arXiv:1901.03338 [astro-ph.HE].

[17] A. van Vliet, R. Alves Batista, and J. R. Hörandel, Phys. Rev. **D100**, 021302 (2019), arXiv:1901.01899 [astro-ph.HE].

[18] R. J. Protheroe and A. P. Szabo, Phys. Rev. Lett. **69**, 2885 (1992).

[19] K. Murase, Y. Inoue, and C. D. Dermer, Phys. Rev. **D90**, 023007 (2014), arXiv:1403.4089 [astro-ph.HE].

[20] X. Rodrigues, A. Fedynitch, S. Gao, D. Boncioli, and W. Winter, Astrophys. J. **854**, 54 (2018), arXiv:1711.02091 [astro-ph.HE].

[21] B. Eichmann, J. P. Rachen, L. Merten, A. van Vliet, and J. Becker Tjus, JCAP **1802**, 036 (2018), arXiv:1701.06792 [astro-ph.HE].

[22] K. Fang and K. Murase, Nature Phys. **14**, 396 (2018), arXiv:1704.00015 [astro-ph.HE].

[23] D. Biehl, D. Boncioli, C. Lunardini, and W. Winter, Sci. Rep. **8**, 10828 (2018), arXiv:1711.03555 [astro-ph.HE].

[24] D. Boncioli, D. Biehl, and W. Winter, Astrophys. J. **872**, 110 (2019), arXiv:1808.07481 [astro-ph.HE].

[25] J. H. Matthews, A. R. Bell, K. M. Blundell, and A. T. Araudo, Mon. Not. Roy. Astron. Soc. **482**, 4303 (2019), arXiv:1810.12350 [astro-ph.HE].

[26] R. Mbarek and D. Caprioli, Astrophys. J. **886**, 8 (2019), arXiv:1904.02720 [astro-ph.HE].

[27] A. Palladino, X. Rodrigues, S. Gao, and W. Winter, Astrophys. J. **871**, 41 (2019), arXiv:1806.04769 [astro-ph.HE].

[28] S. Hümmer, M. Rüger, F. Spanier, and W. Winter, Astro-

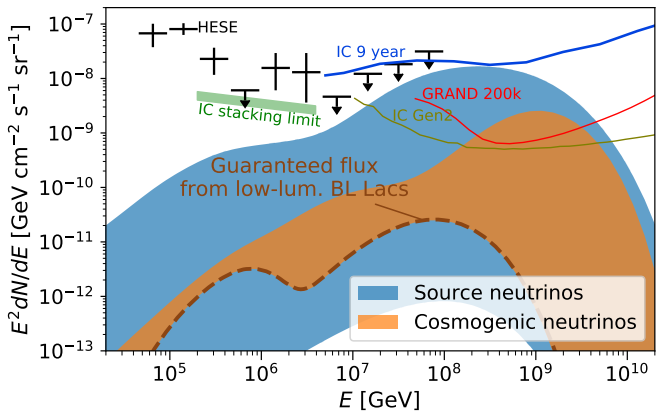

FIG. 3: Predicted (all-flavor) neutrino flux range from the entire blazar population, produced through UHECR interactions inside the sources (source neutrinos, blue region) and during extragalactic propagation (cosmogenic neutrinos, orange region). The neutrino flux can saturate current IceCube limits at EeV energies while avoiding current stacking limits at sub-PeV to PeV energies. This maximum flux would originate mainly in source interactions in FSRQs, with a sub-dominant cosmogenic contribution. At the same time, the contribution from low-luminosity BL Lacs (dashed curve), is a guaranteed (minimal) flux if this source class saturates the UHECR flux as shown in Fig. 2.

phys. J. **721**, 630 (2010), arXiv:1002.1310 [astro-ph.HE].
[29] P. Baerwald, S. Hümmer, and W. Winter, Phys. Rev. **D83**, 067303 (2011), arXiv:1009.4010 [astro-ph.HE].
[30] G. Fossati, L. Maraschi, A. Celotti, A. Comastri, and G. Ghisellini, Mon. Not. Roy. Astron. Soc. **299**, 433 (1998), arXiv:astro-ph/9804103 [astro-ph].
[31] G. Ghisellini, C. Righi, L. Costamante, and F. Tavecchio, Mon. Not. Roy. Astron. Soc. **469**, 255 (2017), arXiv:1702.02571 [astro-ph.HE].
[32] M. Ajello *et al.*, Astrophys. J. **751**, 108 (2012), arXiv:1110.3787 [astro-ph.CO].
[33] M. Ajello *et al.*, Astrophys. J. **780**, 73 (2014), arXiv:1310.0006 [astro-ph.CO].
[34] F. Fenu (Pierre Auger), *The Pierre Auger Observatory: Contributions to the 35th International Cosmic Ray Conference (ICRC 2017)*, , 9 (2017), [PoS(ICRC2017,486(2018)].
[35] J. Bellido (Pierre Auger), *The Pierre Auger Observatory: Contributions to the 35th International Cosmic Ray Conference (ICRC 2017)*, PoS **ICRC2017**, 506 (2018), [,40(2017)].
[36] M. G. Aartsen *et al.* (IceCube), Astrophys. J. **809**, 98 (2015), arXiv:1507.03991 [astro-ph.HE].
[37] M. Ackermann *et al.* (Fermi-LAT), Astrophys. J. **810**, 14 (2015), arXiv:1501.06054 [astro-ph.HE].
[38] A. J. Koning, S. Hilaire, and M. C. Duijvestijn, in *Proceedings, International Conference on Nuclear Data for Science and Tecnology* (2007) pp. 211–214.
[39] B. T. Zhang, K. Murase, S. S. Kimura, S. Horiuchi, and P. Mészáros, Phys. Rev. **D97**, 083010 (2018), arXiv:1712.09984 [astro-ph.HE].
[40] Y. Ohira, K. Murase, and R. Yamazaki, Astron. Astrophys. **513**, A17 (2010), arXiv:0910.3449 [astro-ph.HE].
[41] N. Globus, D. Allard, R. Mochkovitch, and E. Parizot, Mon. Not. Roy. Astron. Soc. **451**, 751 (2015), arXiv:1409.1271 [astro-ph.HE].
[42] R. Alves Batista, A. Dundovic, M. Erdmann, K.-H. Kampert, D. Kuempel, G. Müller, G. Sigl, A. van Vliet, D. Walz, and T. Winchen, JCAP **1605**, 038 (2016), arXiv:1603.07142 [astro-ph.IM].
[43] R. Aloisio, D. Boncioli, A. Di Matteo, A. F. Grillo, S. Petrera, and F. Salamida, JCAP **1711**, 009 (2017), arXiv:1705.03729 [astro-ph.HE].
[44] J. L. Puget, F. W. Stecker, and J. H. Bredekamp, Astrophys. J. **205**, 638 (1976).

APPENDIX A: METHODS

We now discuss in greater detail the methods used in calculating the diffuse flux of UHECRs and neutrinos from the blazar population.

The simulation of UHECR interactions in blazar jets closely follows the methods described by Rodrigues *et al.* [20]. The spectral energy distribution (SED) of each blazar depends only on its gamma-ray luminosity in the *Fermi*-LAT range, following the latest parametrization of the blazar sequence [31], which is based on the recent *Fermi* 3LAC catalog [37]. While this is a simplistic approach for describing the whole blazar population, which may contain different SEDs outside this scheme, it is a computationally accessible approach expected to reproduce a good result if the outliers do not dominate. The luminosity spectrum is converted into an energy density in the jet assuming that cosmic-ray interactions occur in a spherical region (blob) of a given radius. These cosmic rays are assumed to be accelerated somewhere in the blazar jet, and are then injected into this blob where they interact with the photon field.

The blob is assumed to travel with a Doppler factor (from the observer's perspective) of $\delta = 10$. On the other hand, the size of the blob in the co-moving frame of the jet[1], $R'_{\rm blob} = \delta\, R_{\rm blob}$, was kept as a variable parameter whose value was optimized in each example, as described in Appendix B.

The photon spectrum in the blob is considered to be static during the simulation, and we assume it is produced independently by a population of non-thermal electrons that are also accelerated in the jet together with the cosmic-ray nuclei. The magnetic-field strength in the jet is assumed to scale as a power law of the blazar's gamma-ray luminosity, following Appendix A of Ref. [20].

The photo-hadronic interactions of the cosmic-ray nuclei with the photons in the blob are calculated using the NeuCosmA code [28, 29], which consists of a time-dependent solver of a system of partial differential equations that describe the evolution of each particle species involved. This consists of a series of hundreds of nuclear isotopes with masses from hydrogen up to iron-56, photons, pions, muons and neutrinos, which are produced through the decay of these particles. The simulated interactions include pair production, photo-meson production, and photo-disintegration (in the case of nuclei heavier than protons). Photo-disintegration leads to the break-up of nuclear species into lighter elements, and in NeuCosmA this is calculated using the Talys model [38].

The cosmic rays are assumed to be accelerated to a power-law spectrum with an exponential cutoff:

$$\frac{dN}{dE'} \sim E'^{-2} \exp\left(\frac{E'}{E'_{\rm max}}\right), \tag{1}$$

where E' is the energy of the nucleus in the jet rest frame, dN/dE' is the differential energy density of this nuclear species in the jet, and $E'_{\rm max}$ is the maximum injection energy where the cutoff occurs. As mentioned in the main text, the maximum energy of the injected isotopes is calculated self-consistently by balancing the timescales of the acceleration process and the leading cooling process, following the method explained in Ref. [20]. The acceleration timescale depends on the *acceleration efficiency* parameter, $\eta_{\rm acc} \leq 1$, defined as the ratio between the Larmor time of the cosmic rays and their acceleration timescale. Therefore, the value of the acceleration efficiency will determine the maximum energy $E'_{\rm max}$ achieved by each nuclear species in the different sources. The acceleration efficiency was also kept as a variable parameter. However, the range of values scanned in this work were all consistent with Ref. [26] in that they allow for the acceleration of cosmic rays up to ultra-high energies. Compared to Ref. [26], however, we include the possibility that, depending on the parameters, other processes (such as photo-disintegration) may limit the maximum energy.

As discussed in the main text, we fix the relative normalizations of the injection spectra of the different isotopes, motivated by Ref. [26]. Additionally, there is an overall normalization factor that determines how much total power in cosmic rays is accelerated in a blazar. This is given by the *baryonic loading*, defined as the ratio between the total power in accelerated cosmic rays and the gamma-ray luminosity of the source (above 100 MeV). This factor was also kept free in order to have the flexibility of describing cosmic-ray and neutrino flux levels.

The mechanism by which cosmic rays escape from the jet is another factor determining the emitted cosmic-ray spectrum; see Sec. IIIB of Ref. [39] for a detailed discussion. We have considered two possible mechanisms, which are simulated by choosing a different cosmic-ray escape rate $t'^{-1}_{\rm esc}$ as a function of energy. In the example shown in the main text, the cosmic-ray escape rate is given as a log-parabola in terms of the cosmic-ray energy [39–41]

$$\log\left(t'^{-1}_{\rm esc}\,\frac{R'_{\rm blob}}{c}\right) = -\log^2\left(\frac{E'_{\rm CR}}{E'^{\rm max}_{\rm CR}}\right). \tag{2}$$

Thus, at the maximum energy of each cosmic-ray species (calculated with the method described above), its escape rate is maximal and corresponds to free-streaming out of the blob, while at lower cosmic-ray energies, the escape is severely suppressed.

The other tested escape mechanism was advective escape [19], where all cosmic rays can free-stream out of the blob regardless of their energy, $t'^{-1}_{\rm esc} = c/R'_{\rm blob}$. Physically, this corresponds to the scenario where cosmic-ray escape is driven by advection due to, for instance, relativistic winds. None of the best-case scenarios in the all-blazar case explored in the main text use advective escape, but it will be considered in Appendix B where we will discuss alternative scenarios involving only one blazar sub-class at a time, in order to dissect their individual contributions.

The blob radius, acceleration efficiency, baryonic loading and cosmic-ray escape mechanism were the only blazar

[1] We represent variables given in the rest frame of the jet with a primed symbol, and in the observer's frame as unprimed.

properties that were allowed to vary in this work (as detailed in Tab. I in Appendix B). In each simulation these four parameters were considered to be the same across all blazars of any given sub-class: FSRQs, high-luminosity BL Lacs and low-luminosity BL Lacs.

For high-luminosity FSRQs, which are assumed to have large broad-line regions and in some cases a dusty torus, the cosmic rays that escape the jet will continue interacting with external fields of thermal and atomic broad-line emission from these structures. We therefore implement a three-zone model for cosmic-ray escape in these sources. This leads to an additional cooling of the UHECRs and additional neutrino production in these bright FSRQs compared to a BL Lac with the same luminosity. The threshold between a one-zone and a three-zone model is related only to the gamma-ray luminosity of the FSRQ, as detailed in Ref. [20]; see also that reference for further details about the assumptions and the numerical implementation of this model.

The cosmological evolution of blazars follows Ajello *et al.* [32, 33] and is described in terms of a distribution in redshift, luminosity and spectral index (assuming a power-law spectrum in the Fermi-LAT energy window). We integrate the distribution over the spectral index, obtaining a distribution in redshift and luminosity, as shown in Fig. 1. In this description, high-luminosity BL Lacs ($L_\gamma \geq 3.5\times10^{45}$) and FSRQs have positive source evolutions, with a peak around redshift $z = 1$. These objects are quite rare, with typical local densities < 1 Gpc^{-3}. On the other hand, low-luminosity BL Lacs ($L_\gamma < 3.5\times10^{45}$) have a negative evolution with redshift, which means they are most abundant in the local Universe. These objects have local densities higher than the high luminosity ones, with typical values between 1 and 100 Gpc^{-3}.

The simulation of the propagation of UHECRs from their sources to Earth is performed using the PriNCe code. Written in Python, PriNCe uses a vectorized formulation of the UHECR transport equation taking into account the full nuclear cascade due to photodisintegration and photo-meson production, as well as energy losses due to cosmological expansion and pair production. PriNCe has been extensively cross-checked to reproduce results from both CRPropa [42] and SimProp [43]. Photo-disintegration interactions were calculated using the Puget-Stecker-Bredekamp (PSB) parametrization [44]. We adopted the Epos-LHC air-shower model [35] to convert the composition of UHECRs arriving at Earth into values for $\langle X_{\rm max}\rangle$ and $\sigma(X_{\rm max})$. Further details regarding the PriNCe code can be found in Appendix A of Ref. [16].

APPENDIX B: RESULTS (DETAILS)

In the result discussed in the main text, low-luminosity BL Lacs provide the largest contribution to the UHECR spectrum while the other blazar sub-classes play a subdominant role. Here, we explore the possibilities to describe UHECR spectrum and composition data with each individual blazar sub-class separately, keeping the limits on neutrino fluxes in mind. This shows that all of the blazar sub-classes are capable of exhausting the UHECR flux in a part of the energy range, with different associated neutrino fluxes. However, the combined all-blazar scenario explored in the main text gives the best explanation of the UHECR spectrum and composition together. Note that, in order to optimize the results for each specific source class separately, we re-run the parameter scan each time. Therefore, the parameters here are different from the ones that are used for the combined scenario, discussed in the main text; see Table I.

Low-Luminosity BL Lacs: We start by considering cosmic-ray and neutrino emission from low-luminosity BL Lacs only. We define low-luminosity BL Lacs as BL Lacs with a gamma-ray luminosity $L_\gamma \leq 3.5\times10^{45}$ erg/s. The reason for this splitting point is related to their cosmological evolution, as discussed by Palladino *et al.* [27] (see also Fig. 1): BL Lacs below this threshold luminosity are characterized by a negative source evolution, whereas BL Lacs above this threshold luminosity are characterized by a positive source evolution, similarly to FSRQs. This may point towards different characteristics of the BL Lac source classes. We re-run a scan of the source parameters in order to best describe the UHECR spectrum and composition measurements. The result is shown in Fig. 4 and the corresponding parameter set is reported in Tab. I. While the fit to the cosmic-ray spectrum is similar to the main result in Fig. 2, the composition is heavier due to the absence of the proton-rich contribution from more powerful blazars, leading to a worse fit of both $\langle X_{\rm max}\rangle$ and $\sigma(X_{\rm max})$.

The neutrino flux from this source class is relatively low due to the relatively low density of photons inside the source, which makes the photo-hadronic interactions less efficient. For comparison, see the left panel of Fig. 15 of Ref. [20], where the efficiency in neutrino production is reported as a function of the blazar luminosity. The cosmogenic neutrino flux is relatively low as well, because of the negative redshift evolution of low-luminosity BL Lacs. While UHECRs can only reach Earth when they are produced in the local Universe, cosmogenic neutrinos can reach us from much farther away. Closer sources (i.e. for a negative redshift evolution) lead, therefore, to fewer cosmogenic neutrinos arriving at Earth.

High-Luminosity BL Lacs: A high-luminosity BL Lacs only scenario is shown in Fig. 5. Note that the source properties are different from the main result (Fig. 2). In particular, a higher baryonic loading and a more efficient cosmic-ray escape mechanism (advection, *cf.* Tab. I and Appendix A) are implemented here. While the cosmic-ray spectrum is well described above the ankle up to the highest-energies, the composition is too light at high energies. This is due to the high luminosity of these sources, which increases photodisintegration of heavy nuclei inside the sources. Besides $\langle X_{\rm max}\rangle$, the values of $\sigma(X_{\rm max})$ obtained are also too large (bottom right panel). This is due to that, in this scenario, an advective cosmic-ray escape mechanism is necessary to explain the shape of the cosmic-ray spectrum. Cosmic rays are allowed to free-stream out of the source at all energies, leading to a strong mix of emitted isotopes and therefore,

TABLE I: Parameter values of the four blazar parameters that have been tested in this work. The definitions of baryonic loading, acceleration efficiency, blob radius, and cosmic-ray escape mechanism are described in detail in Appendix A. The definitions of the parameters follow Ref. [20]. The parameter values indicated as *main result* correspond to Fig. 2 and Fig. 3. The three bottom rows refer to the alternative parameter sets discussed in Appendix B. In all cases, the mass composition and spectral index of the accelerated cosmic rays, as well as other parameters describing blazar properties, have been fixed.

Example	Blazar class	Baryonic loading	Acceleration efficiency	Escape mechanism	Blob radius [cm]
Main result (all blazars)	LL BL Lacs	11.0	0.1	log-parabola	1.7×10^{17}
	HL BL Lacs	0.2	0.6		2.2×10^{17}
	FSRQs	13.0	0.6		2.2×10^{17}
At and above ankle	LL BL Lacs only	14.4	0.1	log-parabola	1.2×10^{17}
Above-ankle range	HL BL Lacs only	2.6	1.0	advective	3.0×10^{17}
Sub-ankle range	FSRQs only	9.0	0.3	advective	1.3×10^{17}

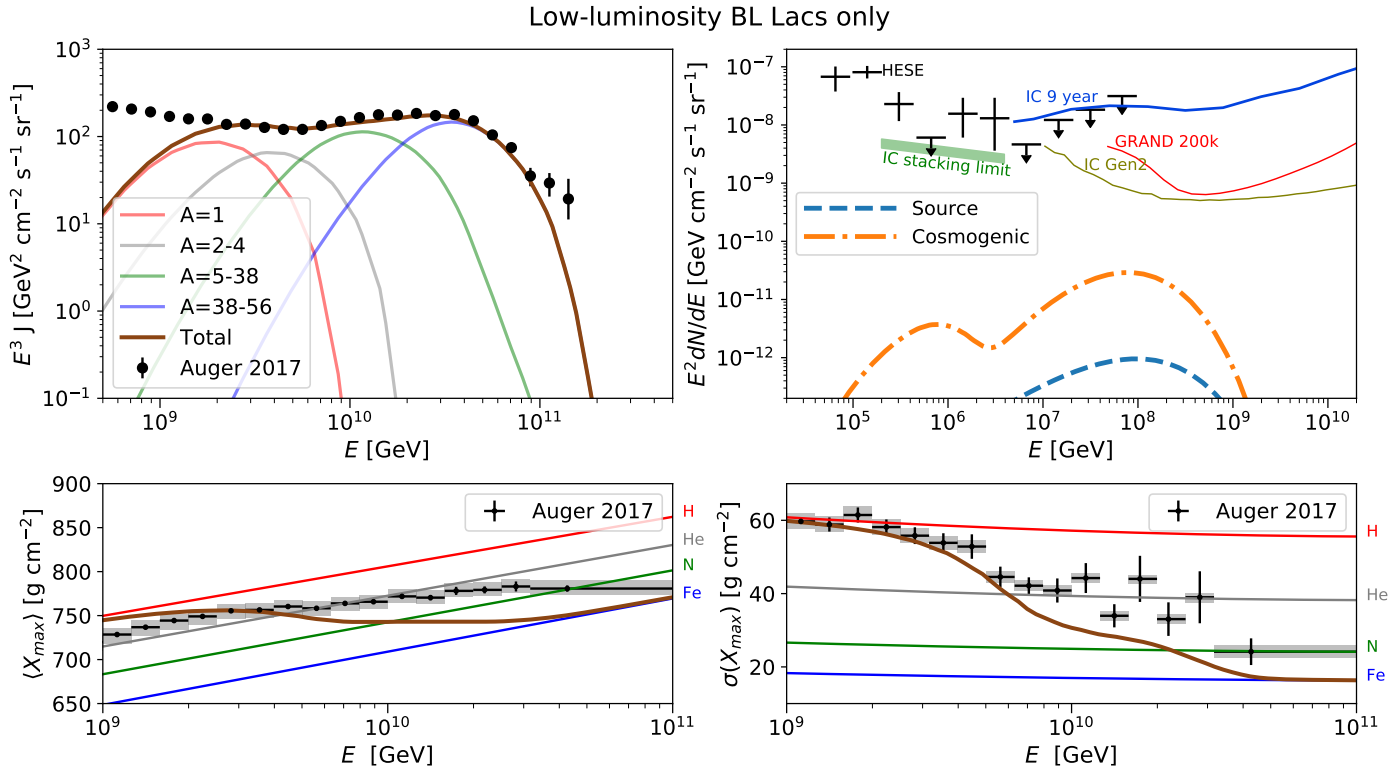

FIG. 4: Expected UHECR spectrum and composition as well as source and cosmogenic neutrino fluxes for a model with only low-luminosity BL Lacs (see Tab. I for simulation parameters). Measured data, limits and expected sensitivities are the same as in Fig. 2. This source class alone can explain the Auger flux in a large energy range at and above the ankle. However, without the contribution from high-luminosity BL Lacs and FSRQs, the overall composition is too heavy to explain the data, yielding a worse result than the main result in Fig. 2 where all blazar classes contribute.

a large variability in the atmospheric showers they initiate. On the contrary, a log-parabola escape rate (as considered for low-luminosity BL Lacs) leads to a rigidity-dependent escape, by predominantly allowing cosmic rays to escape close to their respective maximum energies. This leads to the decrease in $\sigma(X_{\rm max})$ at higher energies observed in Fig. 4, which is necessary to explain the data.

Concerning neutrinos, the expected flux is higher than in the low-luminosity BL Lacs case but lower than in the FSRQs case. This is because the neutrino emission is dominated by BL Lacs with $L_\gamma < 10^{46}$ erg/s. These BL Lacs are abundant but not as efficient as FSRQs in producing neutrinos. On the other hand, high-luminosity BL Lacs are more abundant at high redshifts than low-luminosity BL Lacs (see also Fig. 1), leading to larger source and cosmogenic neutrino fluxes. Moreover, in this scenario a substantial contribution of protons and helium nuclei is present at higher energies – and the cosmogenic neutrino flux increases with lighter nuclei. Note that, although the source neutrino flux is lower than the cosmogenic flux in this case, it may be discriminated by flare or stacking searches.

Flat-Spectrum Radio Quasars: Finally, we consider a scenario where only FSRQs emit UHECRs. In the result discussed in the main text, the cosmic-ray flux from FSRQs was considerably lower than the one from low-luminosity BL Lacs. This was because FSRQs are very efficient neutrino emitters and are, therefore, strongly constrained by current neutrino flux limits (Fig. 2). We now consider a

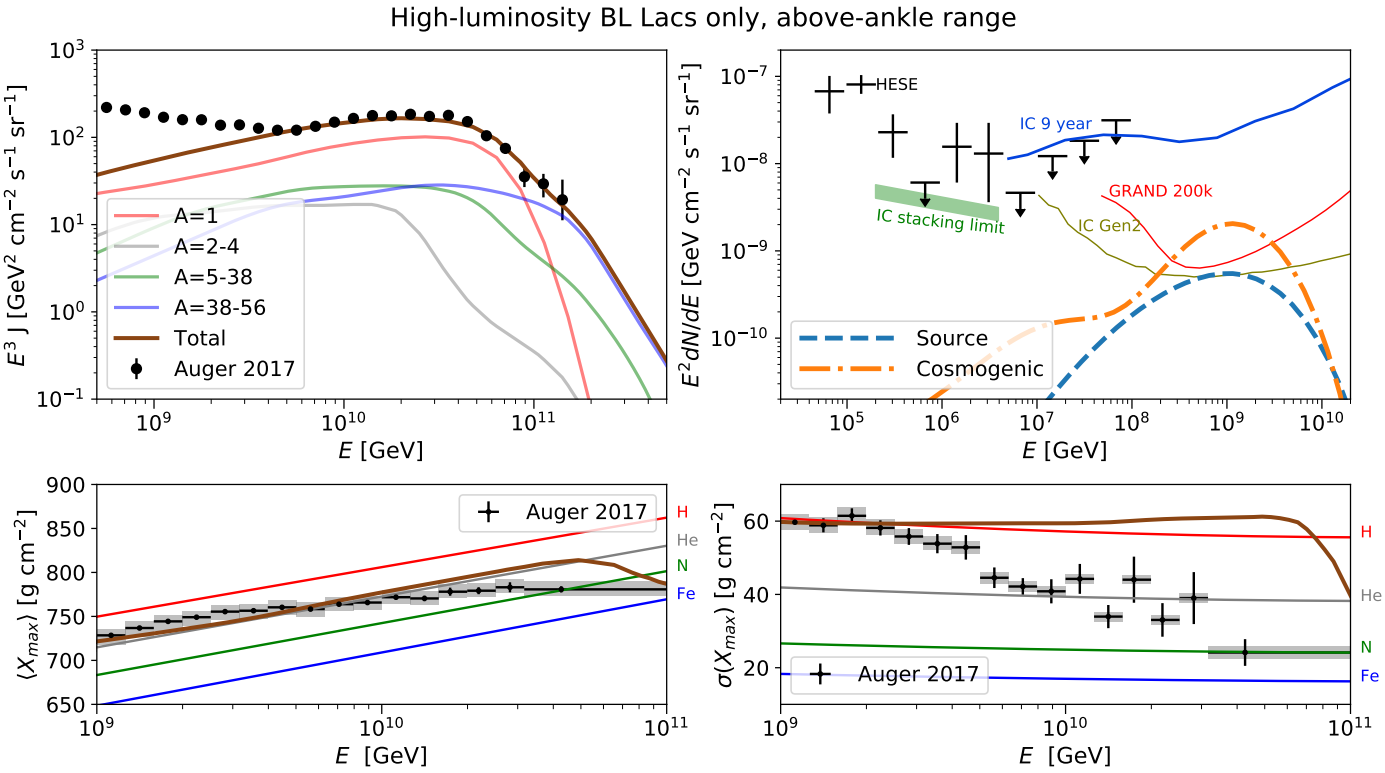

FIG. 5: Expected UHECR spectrum and composition as well as source and cosmogenic neutrino fluxes for a model with only high-luminosity BL Lacs (see Tab. I for simulation parameters). Measured data, limits and expected sensitivities are the same as in Fig. 2. With these parameter values, this source class alone can exhaust the Auger flux above the ankle, while simultaneously emitting a flux of cosmogenic neutrinos in the EeV range that is above the planned sensitivity of IceCube Gen2 and GRAND 200k. However, the emitted UHECR composition is strongly mixed and dominated by light nuclei up to $\sim 10^{11}$ GeV, due to the high luminosity and the advective escape mechanism used in this model. This therefore gives an UHECR composition at Earth which is not compatible with the measured $\sigma(X_{\rm max})$ data by Auger.

different parameter set for FSRQs (bottom line of Tab. I), whose resulting observables are shown in Fig. 6. The acceleration efficiency of FSRQs in this example is lower than in the main result, thus reducing the maximum energy attained by the cosmic rays in the source. Moreover, in this example cosmic rays escape the source through advection. As discussed in Appendix A, this mechanism is *(a)* energy-independent, leading to a softer emission spectrum, and *(b)* more efficient than the log-parabola escape considered in the main text, which means that a source with the same baryonic loading will emit a higher cosmic-ray luminosity. Aspect *(a)*, together with the lower acceleration efficiency, leads to a cosmic-ray spectrum that peaks below the ankle, and strongly softens at ultra-high energies (top-left panel of Fig. 6). At the same time, aspect *(b)* means that cosmic rays from FSRQs can now reach the Auger flux level without violating current IceCube limits (in contrast to the example discussed in main text, where the contribution to the cosmic-ray flux from FSRQs is limited by IceCube limits to less than 10% in the sub-ankle region). In spite of the higher cosmic-ray flux, the baryonic loading of FSRQs in this example is in fact slightly lower than in the main result (*cf.* Tab. I), which demonstrates the effect of the advective escape on the cosmic-ray efficiency of the sources.

While the escape mechanism has a dramatic effect on the cosmic-ray spectrum emitted by blazars, it has minimal impact on neutrino production inside the source itself (see Ref. [20]). On the contrary, the acceleration efficiency does in fact impact in-source neutrino production. In this example, the lower acceleration efficiency reduces the maximum cosmic-ray energies in the source, which leads to the suppression of EeV neutrinos (top-right panel of Fig. 6) compared to the result of Fig. 2. In spite of this, FSRQs in this scenario would still emit a neutrino flux in the EeV range that would be detectable by future radio neutrino experiments.

Finally, we see that the cosmogenic neutrino flux at EeV energies is lower compared to the one expected from high-luminosity BL Lacs only. The reason is that in the case of FSRQs a heavy composition is favored (pure iron at the highest energy), which reduces cosmogenic neutrino production.

Since each exclusive model (one population model) cannot describe UHECR data (spectrum and composition) completely satisfactorily, we present a combination in the main text. In that model, the low-luminosity BL Lacs dominate the UHECR flux with a rigidity-dependent maximum energy and hard (log-parabola) escape spectra, while the other populations help with the description of $\langle X_{\rm max}\rangle$ and $\sigma(X_{\rm max})$. The source neutrino flux is driven by a

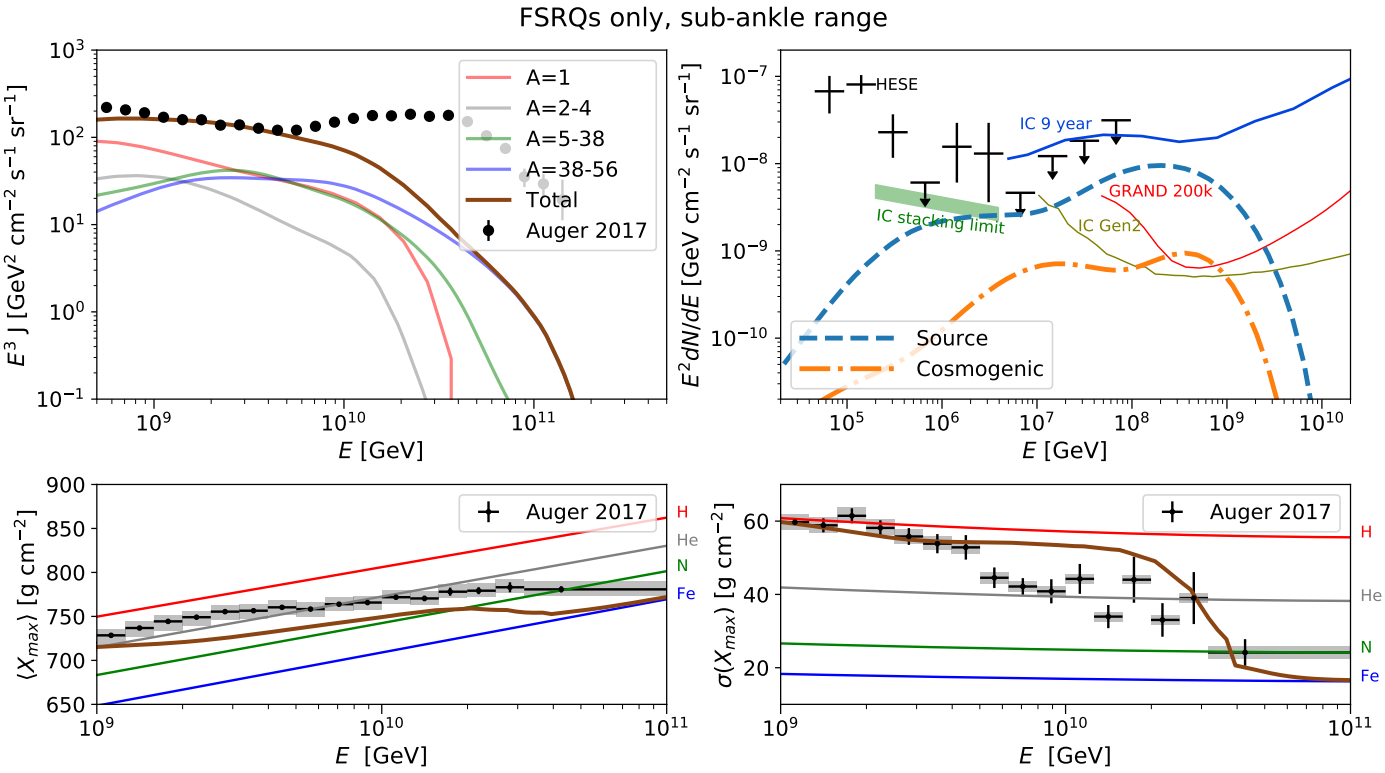

FIG. 6: Expected UHECR spectrum and composition as well as source and cosmogenic neutrino fluxes for a model with only FSRQs (see Tab. I for simulation parameters). Measured data, limits and expected sensitivities are the same as in Fig. 2. The advective cosmic-ray escape mechanism considered here leads to a softer UHECR spectrum that now peaks below the ankle. Since advection is also a more efficient escape mechanism, FSRQs are now better UHECR emitters, which makes them capable of reaching the Auger flux level in this range without violating current IceCube limits on the neutrino flux. Finally, the lower acceleration efficiency in this example reduces the maximum cosmic-ray energies in the source, therefore suppressing the EeV neutrino flux compared to that in Fig. 2.

sub-dominant contribution to the UHECR flux from FSRQs. We emphasize that, while this contribution may be lower for different parameter choices, it cannot be simply switched off without affecting the composition observables. We therefore anticipate that a substantial source neutrino flux could be plausible.